



## Article

# Oxidopamine-Induced Nuclear Alterations Quantified Using Advanced Fractal Analysis: Random Forest Machine Learning Approach

Igor Pantic <sup>1,2,3,4,\*</sup> , Nikola Topalovic <sup>1</sup>, Peter R. Corridon <sup>5,6,7</sup> and Jovana Paunovic <sup>8,\*</sup>

<sup>1</sup> Department of Medical Physiology, Faculty of Medicine, University of Belgrade, Višegradska 26/2, RS-11129 Belgrade, Serbia

<sup>2</sup> University of Haifa, 199 Abba Hushi Blvd, Mount Carmel, Haifa IL-3498838, Israel

<sup>3</sup> Department of Pharmacology, College of Medicine and Health Sciences, Khalifa University of Science and Technology, Abu Dhabi P.O. Box 127788, United Arab Emirates

<sup>4</sup> Department of Physiology and Cell Biology, Faculty of Health Sciences, Ben-Gurion University of the Negev, Be'er Sheva 84105, Israel

<sup>5</sup> Department of Immunology and Physiology, College of Medicine and Health Sciences, Khalifa University of Science and Technology, Abu Dhabi P.O. Box 127788, United Arab Emirates

<sup>6</sup> Biomedical Engineering, Healthcare Engineering Innovation Center, Khalifa University of Science and Technology, Abu Dhabi P.O. Box 127788, United Arab Emirates

<sup>7</sup> Center for Biotechnology, Khalifa University of Science and Technology, Abu Dhabi P.O. Box 127788, United Arab Emirates

<sup>8</sup> Department of Pathophysiology, Faculty of Medicine, University of Belgrade, Dr. Subotića 9, RS-11129 Belgrade, Serbia

\* Correspondence: igor.pantic@med.bg.ac.rs (I.P.); jovana.paunovic@med.bg.ac.rs (J.P.)

**Abstract:** Fractal analysis (FA) is a contemporary computational technique that can assist in identifying and assessing nuanced structural alterations in cells and tissues after exposure to certain toxic chemical agents. Its application in toxicology may be particularly valuable for quantifying structural changes in cell nuclei during conventional microscopy assessments. In recent years, the fractal dimension and lacunarity of cell nuclei, considered among the most significant FA features, have been suggested as potentially important indicators of cell damage and death. In this study, we demonstrate the feasibility of developing a random forest machine learning model that employs fractal indicators as input data to identify yeast cells treated with oxidopamine (6-hydroxydopamine, 6-OHDA), a powerful toxin commonly applied in neuroscience research. The model achieves notable classification accuracy and discriminatory power, with an area under the receiver operating characteristics curve of more than 0.8. Moreover, it surpasses alternative decision tree models, such as the gradient-boosting classifier, in differentiating treated cells from their intact counterparts. Despite the methodological challenges associated with fractal analysis and random forest training, this approach offers a promising avenue for the continued exploration of machine learning applications in cellular physiology, pathology, and toxicology.

**Keywords:** fractal dimension; nucleus; artificial intelligence; toxicology; cell damage



**Citation:** Pantic, I.; Topalovic, N.; Corridon, P.R.; Paunovic, J. Oxidopamine-Induced Nuclear Alterations Quantified Using Advanced Fractal Analysis: Random Forest Machine Learning Approach. *Fractal Fract.* **2023**, *7*, 771. <https://doi.org/10.3390/fractalfract7100771>

Academic Editor: Sergei Fedotov

Received: 11 September 2023

Revised: 19 October 2023

Accepted: 20 October 2023

Published: 23 October 2023



**Copyright:** © 2023 by the authors. Licensee MDPI, Basel, Switzerland. This article is an open access article distributed under the terms and conditions of the Creative Commons Attribution (CC BY) license (<https://creativecommons.org/licenses/by/4.0/>).

## 1. Introduction

Fractal analysis (FA) is a contemporary computational method that is frequently applied for quantifying complex structures and phenomena. In biology and medicine, in some circumstances, it may be applied for signal analysis and classification, as well as in addition to conventional image analysis tools [1,2]. For two-dimensional signals such as radiological or microscopic images, FA can provide valuable insights into their statistical properties. For example, small changes in textural patterns in digital micrographs, such as alterations in roughness and other fine-scale features, often invisible during standard microscopy, can be detected with FA features. This may enable the researcher to adequately

classify different textural patterns of tissues and cells and predict various physiological and pathological phenomena [3,4].

Fractal quantifiers can be used as input data for training and testing of various supervised machine learning models [5–7]. In these approaches, the machine is presented with a series of examples where inputs are fractal indicators such as the values of fractal dimension and lacunarity. The output data may include categorical variables representing an assigned class (of a patient, tissue, cell, etc.), or a continuous variable such as a blood concentration of a certain substance. In recent years, many research efforts have been focused on decision tree ML algorithms that utilize a hierarchical data structure resembling a tree to make the decision on some prediction or classification. These models range from relatively simple ones based on the CART (classification and regression trees) algorithm and gradient-boosting classifiers to more complex random forests.

Random forest (RF) algorithms are particularly intriguing supervised learning ensemble methods that are today commonly used in medical data analysis due to their versatility and accuracy [8–11]. They combine information from a multitude of individual decision trees that are created to include a randomly chosen subset of a training data sample. When a random forest model is used for classification tasks (i.e., separating cells into classes of damaged and intact cells), the class is determined by majority voting based on the collective outputs of decision trees. Random forests are capable of detecting non-linear relationships which can be useful in signal analysis in molecular and cell biology. In microscopy, these models are particularly useful in handling high-dimensional data that may be the product of complex image analyses of digital micrographs. During the evaluation of data obtained from light microscopy, RFs can quantify feature importance and identify a microscopic feature that best contributes to the observed structural changes. Also, these models are characterized by a high degree of robustness to overfitting which is potentially valuable in large and versatile microscopy data frames [9,12].

In previous research, it was shown that exposure to oxidopamine (6-hydroxydopamine) may induce discrete structural changes in yeast cell nuclei, quantifiable using advanced computational techniques for generating data to train random forest models [5,13]. Oxidopamine is a powerful toxin which, under certain circumstances, increases the production of reactive oxygen species, leading to oxidative stress. Under specific experimental conditions, it can cause DNA damage and activate various damage response pathways in the cell nucleus. In some cells, it can also lead to numerous gene expression and epigenetic changes, which may contribute to the loss of certain physiological functions and programmed cell death. In our recent research, we have indicated that it might be possible to use random trees and random forest algorithms to detect discrete structural changes in cell nuclei after exposure to oxidopamine. By using advanced fractal analysis and its features, such as fractal dimension and lacunarity, we were able to train and test the random forest model with solid classification accuracy and discriminatory power in differentiating oxidopamine-treated cells from intact ones. We also show that the random forest model may outperform the alternative classification and regression tree (CART) model, as well as the gradient-boosting classifier in terms of its ability to classify treated and control cells.

## 2. Materials and Methods

The experimental part of the research was performed on *Saccharomyces cerevisiae* yeast cells similar to the ones utilized in the previously published work [5]. Briefly, the cells were kept in yeast extract peptone–dextrose (YPD) broth and incubated in an orbital shaker with agitation at 200 rpm and kept at 25 °C and pH 6.5. The treatment of the cells was done in specialized tissue chambers/slides (REF). Cells were exposed to oxidopamine (6-hydroxydopamine, 6-OHDA) at a dose of 300 µM for 120 min, an exposure previously shown to significantly induce changes in textural (gray-level co-occurrence matrix) indicators [13]. As mentioned in the previous publication, the genetic information of *Saccharomyces cerevisiae* may be found at the European Nucleotide Archive (ENA) and other databases. The cells were partially fixated in methanol and exposed to Giemsa nucleic

acid stain composed of compounds Azure B, methylene blue, and eosin. In eukaryotes, this stain is known to be specific to DNA phosphate groups and parts of DNA rich in adenine-thymine bonding.

Digital micrographs of the cells were created separately for the treated and control cells using a TCA1000-C instrument (COLO LabExperts, Novo Mesto, Slovenia) with an Aptina MT9J003 CMOS sensor (COLO LabExperts, Novo Mesto, Slovenia). The instrument was mounted on an OPTIC900TH Trinocular Biological Microscope (COLO LabExperts, Novo Mesto, Slovenia). The dimensions of the micrographs were 1600 pixels (width) and 1200 pixels (height) and the bit depth was set to 24. Both vertical and horizontal resolutions were set to 96 dots per inch. Using the ImageJ software (v. 1.53t), freehand regions of interest (ROIs) of cell nuclei were created and saved to the ROI manager. We analyzed a total of 1000 ROIs of oxidopamine-treated and 1000 ROIs of control cells (Figure 1).

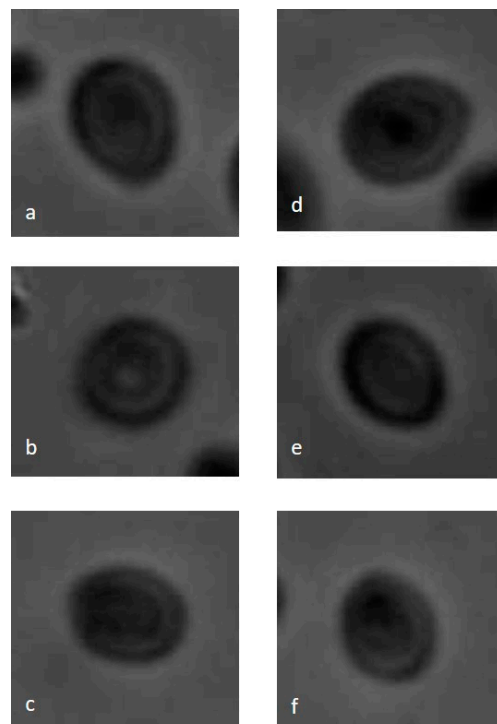


**Figure 1.** Intact *Saccharomyces cerevisiae* cells (a–c) compared with oxidopamine-treated cells (d–f). Despite visual similarities, the two groups show significant differences in nuclear fractal dimension and lacunarity, as observed through both conventional and differential volume variation approaches to fractal analysis.

Fractal analysis of nuclear ROIs was performed in ImageJ (v. 1.53t, developed by Wayne Rasband and contributors, National Institutes of Health, Bethesda, MD, USA), and FracLac software for ImageJ designed by Dr. Audrey Karperien, the Charles Sturt University, Australia [14]. The details on the ImageJ software and its functions can be found in the previously published work [15]. This platform can efficiently compute a number of fractal indicators for a specified structural pattern in a digital image and has been previously used on numerous occasions in biomedical research [16–18]. We applied the box-counting method, in which a grid of boxes (two-dimensional squares) is superimposed over a pattern after which the program counts the number of boxes (N) that contain a part of the pattern. The process is repeated at different scales ( $\epsilon$ ), with different box sizes, after which a log-log graph is created representing the relationship between the box numbers and scales (Figure 2).

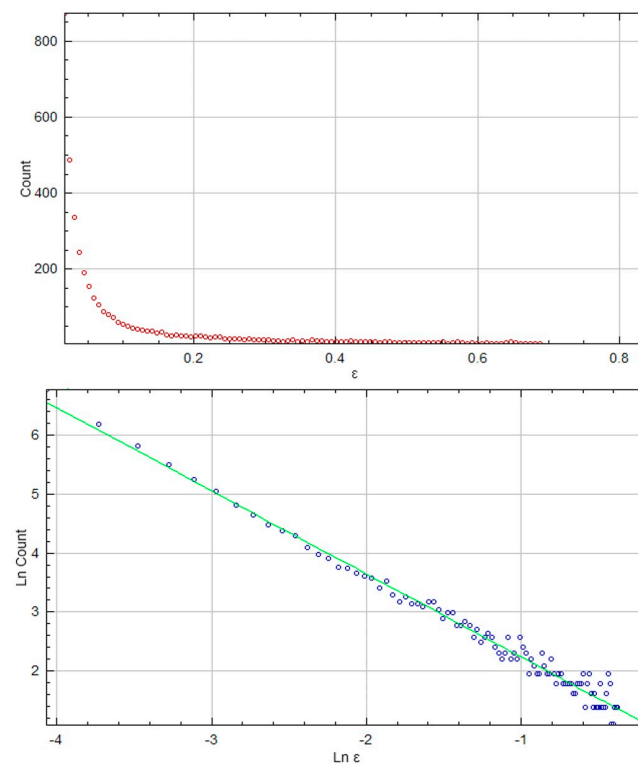


**Figure 2.** Illustration of the regression line creation for fractal dimension calculation in FracLac software. A grid of two-dimensional squares is overlaid on a pattern, and the software counts the boxes ( $N$ ) containing part of the pattern. This process is repeated with varying box sizes ( $\epsilon$ ), leading to a log-log graph that captures the relationship between box counts and scales.

The value of the fractal dimension ( $D_B$ ) is calculated from the slope of the regression line in the log-log graph:

$$D = \lim_{\epsilon \rightarrow 0} [\log N_{\epsilon} / \log \epsilon]$$

Lacunarity as a measure of rotational and translational invariance of the nuclear ROI was calculated from the variation coefficient for pixel mass.

$$\lambda = CV_{\epsilon,g}^2 = (\sigma_{\epsilon,g} / \mu_{\epsilon,g})^2$$

where  $g$  is the grid position and  $\sigma$  is the standard deviation.

In this work, we calculated the mean values of fractal dimension ( $D_{bin}$ ) and lacunarity  $\lambda_{bin}$  in nuclear ROIs that were automatically binarized by FracLac software (version 2015Sep090313a9330). Binarization was achieved utilizing the subsequent option/setting: FracLac > BC > Image Type > Autoconvert to binary. The program automatically designated the foreground based on the relative pixel count within the analyzed object. This facilitated the automatic thresholding of images using ImageJ's inherent function. For detailed information regarding binarization and thresholding, readers are directed to the FracLac software documentation [14]. In addition to this conventional fractal analysis, we also performed analysis on non-binarized grayscale micrographs using the so-called "Differential Volume Variation" technique. This method includes the definition of three-dimensional volumes ( $V_{i,j,\epsilon}$ ) over a two-dimensional space, and the same applies to individual boxes and resolution units [14]. The volumes are proportional to box sizes, shapes, and detected intensities:

$$V_{i,j,\epsilon} \sim I_{i,j,\epsilon} * \epsilon^2$$

The slope of the regression line is calculated as

$$S = \lim_{\epsilon \rightarrow 0} (\ln V_{\epsilon} / \ln 1/\epsilon)$$

where

$$V\epsilon = \sum I_{ij,\epsilon} \epsilon^2$$

Finally, the value of fractal dimension ( $D_{\text{dif}}$ ) is calculated as

$$D_{\text{dif}} = 3 - (S/2)$$

Lacunarity using the differential method ( $\lambda_{\text{dif}}$ ) was calculated based on the ratio of the variance of the local difference of pixel intensities to the square of the mean of the differences.

The calculated nuclear fractal dimensions and lacunarities were used as input data for the training of decision tree models. We trained and tested a model based on the conventional CART (classification and regression tree) algorithm, a model based on the gradient-boosting ensemble learning method, and a model based on the random forest algorithm. For all three models, a sample of 2000 nuclear ROIs was used and it was divided such that 80% was used for training and the remaining 20% for testing (80/20 split). The division of the training and testing sets was done similarly to a previously published study on the same cell type, where a random forest model was successfully developed and tested using textural features as input data [5]. Additionally, we trained and tested the models using two alternative divisions: 70/30 and 90/10. All three models were developed in scikit-learn, an open-source Python machine learning library [19]. Data preprocessing, summarization, and exploration were done in Pandas data analysis and manipulation library for Python, while statistical analysis was done in SPSS (v.25, IBM Corporation, Chicago, IL, USA). Multivariate analysis of variance was used for testing the difference between the groups. A  $p$ -value of less than 0.05 was considered to be statistically significant.

The classification and regression tree (CART) model was used to optimize the maximum homogeneity within each subset of the data following binary recursive partitioning. For the purposes of our research, we used the Gini impurity criterion to establish the frequency of incorrect classification of a randomly selected data element. The model evaluated each split for the fractal features subsequently selecting the split associated with the lowest Gini impurity. On the other hand, the gradient-boosting model was developed by building an ensemble of decision trees in a sequential manner with trees later in line correcting the errors of the earlier trees. The model was focused on these residual errors and forming the steepest descent direction (gradient descent) after which the optimization of the loss function was performed. The weighted sum of the predictions of individual trees was taken into account when making the final predictions.

The random forest classifier was developed in a similar way to the above-mentioned models, using fractal dimension and lacunarity data as inputs and the class of the cell (damaged or intact) as the target. As previously mentioned, this supervised learning ensemble method combines information from a multitude of individual decision trees that are created to include a randomly chosen subset of a training data sample. Our model applied the principles of bootstrap aggregating (bagging) to ensure randomness and variability of the trees, as well as feature randomness for a higher degree of variation during node splitting. These approaches significantly reduced the probability of overfitting. Majority voting based on the collective outputs of decision trees was used in making final predictions. In our work, we integrated the hyperparameter tuning process using the 'GridSearchCV' tool in the 'scikit-learn' library in Python.

We have evaluated all 3 machine learning models by calculating the classification accuracy using the 'accuracy\_score' function from scikit-learn. For the evaluation of the discriminatory power of the models, we conducted a receiver operating characteristic (ROC) analysis. The ROC analysis was done after model fitting using the 'predict\_proba' method which returned the probabilities for each class. The ROC curve was computed using the 'roc\_curve' function from the 'scikit-learn' library and the area under the curve was quantified using the 'roc\_auc\_score' function. The curve was displayed using 'matplotlib',

a comprehensive library for creating mathematical visualizations in Python, showing the trade-offs between sensitivity and specificity for different decision thresholds.

### 3. Results

The average values of fractal dimension obtained from binarized ROIs using the standard box-counting method were  $1.469 \pm 0.183$  in the oxidopamine-treated group and  $1.594 \pm 0.144$  in the control group of cells (Figure 3). A statistically highly significant difference ( $p < 0.01$ ) was observed between the groups. The mean values of lacunarity in the binarized ROIs in the control group was  $0.548 \pm 0.179$ , while in the oxidopamine-treated group, it significantly increased to  $0.706 \pm 0.208$  ( $p < 0.01$ ). When we applied the fractal analysis on non-binarized grayscale micrographs using the so-called “Differential Volume Variation” technique, we observed a similar reduction of fractal dimension and an increase in lacunarity values. The mean value of fractal dimension in the experimental group was  $2.609 \pm 0.044$  and it was significantly ( $p < 0.01$ ) lower when compared to the controls ( $2.665 \pm 0.053$ ). The average lacunarity in the controls was  $0.258 \pm 0.175$  and in oxidopamine-treated cells  $0.491 \pm 0.253$  ( $p < 0.01$ ).

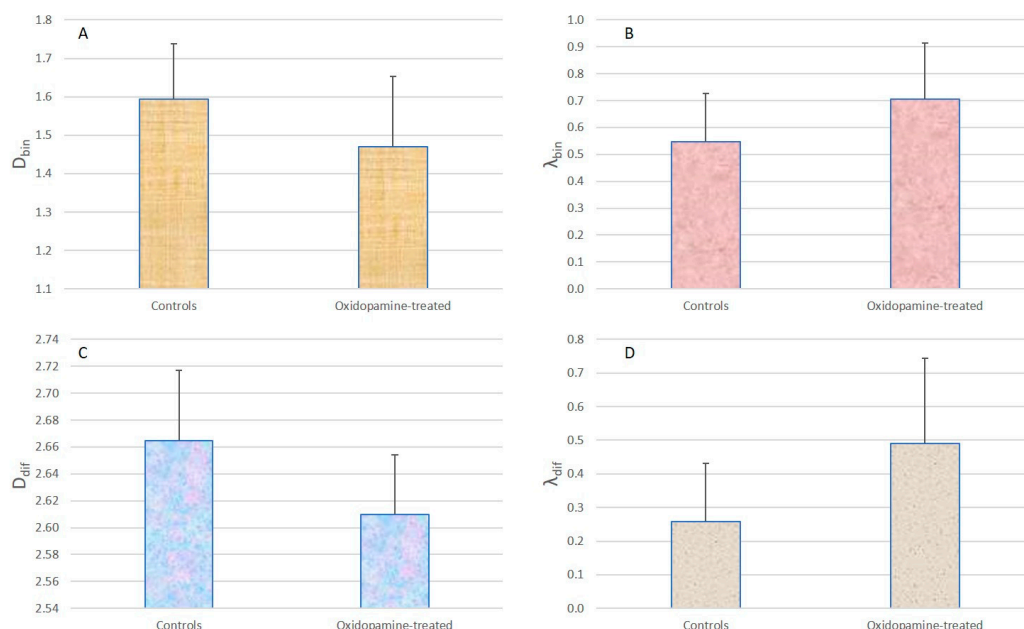


**Figure 3.** Graphs (A,B) display the average values of nuclear fractal dimension and lacunarity ( $D_{bin}$  and  $\lambda_{bin}$ , respectively) derived from binarized regions of interest (ROIs) via the standard box-counting method. Conversely, graphs (C,D) show the average values ( $D_{dif}$  and  $\lambda_{dif}$ , respectively) obtained from grayscale ROIs using the differential volume variation approach.

The classification accuracies of the classification and regression tree (CART) model for 80/20, 70/30, and 90/10 splits were 67.7%, 65.3%, and 64.2%, respectively (average of 65.7%), and the area under the ROC curve was estimated to be 0.76, 0.74, and 0.74, respectively (average 0.75 for testing samples, 0.81 for training samples, Figure 4). We observed a sensitivity of 60.3% and a specificity of 75.3%. The Matthews correlation coefficient equaled 0.36 and the area under the precision–recall curve was determined to be 0.68. After feature importance analysis was performed (using the ‘feature\_importances’ attribute of the trained CART classifier) it was determined that the differential volume variation lacunarity had the highest score of 0.73. The scores for other input parameters were much lower with differential volume variation fractal dimension having a score of 0.08. Fractal dimension and lacunarity determined by the standard box-counting method on binarized ROIs had feature importance scores of 0.06 and 0.14, respectively. The F1 score, calculated using the ‘f1\_score’ function was calculated to be 0.65 indicating a moderate



performance in terms of balance between the precision and the recall of the model. After the optimization of hyperparameters, it was determined that the best hyperparameters were 'criterion' 'gini'; 'max\_depth' 3; 'min\_samples\_leaf' 1, and 'min\_samples\_split' 2.

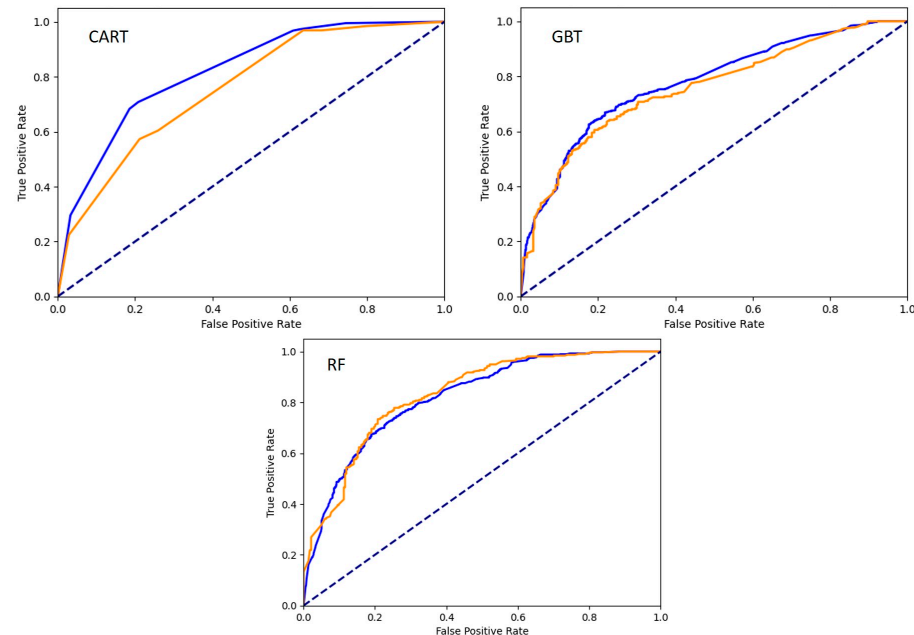


**Figure 4.** Receiver operating characteristic curves for the classification and regression tree (CART) model, gradient-boosting tree (GBT) model, and random forest (RF) classifier.

The gradient-boosting tree model had classification accuracies for 80/20, 70/30, and 90/10 splits of 69.7%, 67.5%, and 66.9% (average 68.0%) while the area under the ROC curve equaled 0.76, 0.75, and 0.74 (average 0.75, for training sample 0.77). We observed a sensitivity of 67.8% and a specificity of 71.6%. The Matthews correlation coefficient equaled 0.39 and the area under the precision–recall curve was determined to be 0.73. Feature importance analysis (again, using the 'feature\_importances' attribute) showed that similarly to the CART model, the differential volume variation lacunarity had the highest score of 0.496, followed by the differential volume variation fractal dimension score of 0.32. Fractal dimension and lacunarity obtained using the conventional methodology had feature importance scores of 0.13 and 0.05, respectively. The F1 score of the machine learning model was 0.69. After the optimization of hyperparameters, it was determined that the best hyperparameters were 'learning\_rate' 0.1, 'max\_depth' 3, 'min\_samples\_leaf' 2, 'min\_samples\_split' 6, 'n\_estimators' 50, and 'subsample' 0.9.

The random forest model outperformed both the CART and the gradient-boosting tree model since its classification accuracy was determined to be 76.1% for the 80/20 data split while for the 70/30 and 90/10 splits it equaled 74.7% and 74.3% (average 75.0%). The area under the curve of the model for the testing set, for 80/20, 70/30, and 90/10 splits were 0.83, 0.82, and 0.82, respectively (average 0.82), indicating a very good discriminatory power in differentiating nuclear ROIs from treated cells from the controls. Similar AUC values, on average 0.82 were observed for the training sets. We observed a sensitivity of 73.1% and a specificity of 79.2%. The Matthews correlation coefficient equaled 0.52 and the area under the precision–recall curve was determined to be 0.74. Lacunarity calculated using the differential volume variation method had the highest feature importance score of 0.45 closely followed by the differential volume variation fractal dimension score of 0.36. In other words, although the model relied on the lacunarity feature, the fractal dimension also played a significant role in the decision-making process. Fractal dimension and lacunarity calculated by conventional means had lower feature importances of 0.08 and 0.11, respectively. The F1 score of the random forest model was significantly higher

when compared to the CART and gradient-boosting tree models and it equaled 0.76. This indicated that the RF model had a relatively high harmonic mean of precision and recall, at least when compared to other approaches. After the optimization of hyperparameters, it was determined that the best hyperparameters were ‘max\_depth’ None; ‘min\_samples\_leaf’ 2; ‘min\_samples\_split’ 5, and ‘n\_estimators’ 50.

#### 4. Discussion

Random forest models have potentially significant applications in the fields of microscopy and cell biology [20]. They can be trained to provide substantial contributions to the proper segmentation of cells and their nuclei with the ability to distinguish boundaries in tissue and culture images. Random forest models can also be used for cell classification which can be particularly useful when there is a need to separate normal from pathologically changed cells [8]. The best examples would be the application of RF to distinguish cancer cells based on their unique multi-scale structural features, and in some cases, the classification accuracy of these models may be quite high. It should be noted that these structural features are also commonly observable during standard microscopy so the high discriminatory power of RF is expected. In contrast to these approaches, our research was focused on the structural changes that were induced by sublethal toxin doses and not visible during conventional histopathological evaluation.

In this research, we focused on the two most important features of fractal analysis—fractal dimension (FD) and lacunarity. When analyzing a tissue or cell micrograph, fractal dimension refers to the level of intricacy and roughness. More complex biological structures tend to exhibit higher values of this parameter, although this greatly depends on the nature of the structure being analyzed, experimental conditions, and the type of fractal dimension being calculated [21–23]. Indeed, there are several different types of fractal dimensions that can be utilized in biological and medical sciences. Standard box count FD of binarized images such as digital micrographs is frequently determined in biomedicine by counting the number of boxes superimposed over a binarized image (or region of interest) at different scales, and subsequent construction of a regression line on a logarithmic graph representing the number of boxes and the scale. This type of FD is determined from the slope of the regression line and is often used to assess the complexity and irregularity of the binarized structure, roughness, branching patterns, and other phenomena. In contrast to the fractal dimension, lacunarity refers to the distribution and size of gaps in the analyzed structural pattern over different scales. Homogeneous systems with uniform or clustered distribution of structural voids tend to have relatively low values of this parameter [16,18].

In our work, we employed a novel methodology for acquiring fractal data which, to the best of our knowledge, has not been previously utilized to generate input data for random forest (RF) model training. Fractal dimensions and lacunarities were ascertained through two distinct approaches: binarization and grayscale conversion. The binarization approach enables straightforward characterization of regions of interest (ROIs) by classifying them into two distinct categories. However, this technique often results in the loss of substantial information from the original image, attributed to the diminishment of geometric attributes, among other factors. In contrast, the grayscale approach analyzes non-binarized grayscale ROIs, which, with their multiple intensity levels, facilitate a more nuanced and detailed representation of structures. The grayscale method might also exhibit heightened sensitivity to intensity variations in complex structures, such as cell nuclei. It is imperative to highlight that besides the binary vs. grayscale distinction, there exist other significant methodological differences between the two approaches implemented in our study. Unlike the binarization method, the grayscale technique employed “Differential Volume Variation” analysis, incorporating the definition of three-dimensional volumes ( $V_{i,j,\epsilon}$ ) over a two-dimensional space. Consequently, notable disparities in the values of fractal dimensions and lacunarities derived from these two methods are anticipated.



In a previously published work [5], a similar approach was applied in order to create random forest and support vector machine models capable of detecting nuclear patterns of yeast cells exposed to a hyperosmotic environment. As input data, the authors used the values of fractal dimension, features of gray-level co-occurrence matrix statistics as well as the features of the discrete wavelet transform. The random forest model had a classification accuracy of 79.8%, outperforming the support vector machine which had an accuracy of 71.7%. The work also demonstrated that it was feasible to create an RF model that uses versatile quantifiers of nuclear texture in order to predict the discrete structural stress in cells which is generally not observable during standard light microscopy assessment. However, it is difficult to adequately compare these results to the findings of our current study due to the substantial methodological differences which include the use of Giemsa stain, specific visualization and image acquisition settings, and the unique technical approach in the quantification of fractal indicators in ROIs of oxidopamine-treated cells.

This is not the first research to induce sublethal cell damage in *Saccharomyces cerevisiae* using oxidopamine. Previously, after exposure to a similar dose of this toxin, it was shown that in a relatively short time period, substantial change in nuclear texture takes place and that this change cannot be visualized even by an experienced expert in the field of microscopy [13]. Texture was assessed using a gray-level co-occurrence matrix algorithm, a second-order statistical technique known for its ability to identify subtle alterations in cell and tissue structure. Treatment with oxidopamine was associated with a statistically significant rise in nuclear textural contrast and variance, while at the same time indicators of textural local homogeneity and uniformity such as angular second moment and inverse difference moment were reduced. The results of our current research are at least partially in line with these findings since it may be expected that the chemical agent that increases the level of textural disorder may subsequently lead to the loss of structural complexity in the biological system.

Oxidopamine is considered to be a potent neurotoxin and is today commonly used for the creation of animal laboratory models of Parkinson's disease and other neurological disorders [24–27]. Although its primary mechanism of action relies on its affinity to dopaminergic neurons, it also exhibits various forms of toxicity in other cell types. In yeast cells, it may induce oxidative stress, activate various stress response pathways, and cause cell cycle arrest due to DNA damage. Oxidative stress in general can be caused due to several processes that are related to the generation of reactive oxygen species including changes in redox cycling, mitochondrial dysfunction, protein oxidation, and lipid peroxidation [28–31]. All of these factors can directly or indirectly cause changes in gene expression in the cell nuclei that can at least partially reflect the changes in chromatin distribution and organization. These subtle changes in chromatin structure could have been associated with the observed changes in fractal indicators. This would be in accordance with previous assumptions that minor alterations in euchromatin and heterochromatin distribution may affect the level of complexity of the nuclear structure.

Although the focus of our research was not to investigate molecular mechanisms of oxidopamine action in yeast, we could speculate that in this case changes in nuclear fractal indicators could have been associated with cell signaling that occurs during early stages of apoptosis. Oxidopamine is indeed a proapoptotic agent in some cell types while, on the other hand, programmed cell death is sometimes associated with complexity loss, reduction of cellular fractal dimension, and increase in nuclear lacunarity. In certain experimental conditions, changes in fractal indicators are potentially valuable indicators of subtle structural changes preceding apoptosis and are sometimes even more sensitive in the detection of apoptosis than conventional cytofluorometric methods. However, it should be noted that at present, fractal analysis is neither frequently used nor a reliable method for apoptosis evaluation in microscopy and that this hypothesis needs to be confirmed by future research.

The integration of fractal analysis with machine learning approaches such as random forests enhances the potential for future development of a sensitive artificial intelligence

(AI)-based biosensor, applicable in both biology and medicine for research and clinical work. Using properties derived from fractal geometry as input data during the training of machine learning models offers an innovative way to enhance the robustness of narrow artificial intelligence systems currently being considered in the field of pathology. The scale-invariant nature of fractal measures further increases their potential value in specimen analysis within digital pathology, given that the complexity of many biological structures may remain consistent across various magnifications. The incorporation of fractal indicators into AI models, based on random forest or other decision tree architectures, may contribute to the future creation of computer-aided diagnostic systems that could significantly benefit current practices in clinical medicine. This becomes especially crucial, considering that current pathohistological diagnoses often rely solely on the subjective opinions of experts, rather than objective calculations and quantifications. This subjective approach occasionally leads to an increased probability of diagnostic errors. These errors have far-reaching impacts on pathology, as they play a crucial role in determining therapeutic decisions and strategies.

However, despite the obvious strengths of our approach, our study had several limitations that may substantially hamper the impact of its findings in biomedicine. Application of fractal measures in random forest model development can be computationally intensive especially since it often requires a large number of calculations on high-quality micrographs or regions of interest. Results on fractal indicators also often significantly vary across different computational platforms, and different programs for calculation of fractal dimension, despite using the same methodology, often yield different outputs [14,16–18]. Furthermore, from our own experience and based on literature data, indicators such as fractal dimension and lacunarity greatly depend on the type of staining, the protocol used during image acquisition (i.e., white balance, contrast, hue, etc.), and even the small manipulations during the fine-tuning of the focus during microscopy.

Another significant limitation of our research is the utilization of only one oxidopamine concentration to induce changes in nuclear structure. This concentration, demonstrated in previous work, affects the properties of nuclear texture quantified by the gray-level co-occurrence matrix computational method without substantially altering the visual characteristics of the nuclei under conventional microscopy [13]. Nonetheless, further research is needed to determine whether the observed reduction in fractal dimension and increase in lacunarity are dose-dependent. Moreover, future investigations should establish the minimal oxidopamine dose required to train, test, and deploy an accurate machine learning model effectively.

Finally, it should be noted that the random forest machine learning model itself often suffers from a lack of interpretability, and understanding the decision-making process within the model is often difficult, if not impossible. The complexity resulting from combining a large number of decision trees leads to the inability to explain the inner workings of the model and therefore, these ML types are often referred to as “black boxes” in scientific computing [32]. Hopefully, in the future, by defining and implementing rigorous research protocols, and with further development of AI technology, we will be able to overcome most of these limitations.

In the future, one could foresee that this type of integration of fractal analysis with machine learning might be further improved for the creation of advanced and innovative biosensors for detecting cell damage in various experiments and even in clinical conditions. New technologies, such as the use of advanced computer chips and the additional inclusion of large data repositories for model training, could be used to alleviate the problem of computational complexity in this field. Also, one should stress the potential importance of alternative machine learning methods, such as the ones based on transfer learning and convolutional neural networks (CNNs). In this work, we focused on the application of decision tree algorithms because, in the past, they have been successfully applied for detecting this type of structural change in yeast cell nuclei [5]. Nevertheless, it may well be possible that CNN and other similar deep learning approaches may, in the future, yield even better classification performance and discriminatory power. This is especially true,

having in mind today's wide applications of CNNs in computer vision, and previously published works that indicate the usefulness of deep learning algorithms, such as multilayer perceptrons, in the microscopic analysis of yeast cells [33].

## 5. Conclusions

Our results demonstrate that it is possible to create a random forest machine learning model that utilizes fractal indicators as input data for the identification of oxidopamine-treated yeast cells. With acceptable classification accuracy and discriminatory power, the model can detect subtle structural alterations in cell nuclei previously exposed to Giemsa nucleic acid stain. It also outperforms alternative decision tree models, such as the gradient-boosting classifier, regarding the ability to separate treated cells from intact ones. Despite significant methodological limitations related to fractal analysis and random forest training, this model provides a potentially valuable basis for further exploration of machine learning strategies in the fields of cellular physiology, pathology, and toxicology.

**Author Contributions:** Conceptualization: I.P., J.P. and P.R.C.; methodology: I.P.; software: I.P.; resources: N.T.; data curation: I.P. and N.T.; writing—original draft preparation: I.P., J.P., N.T. and P.R.C.; writing—review and editing: I.P., J.P., N.T. and P.R.C. All authors have read and agreed to the published version of the manuscript.

**Funding:** This research was supported by the Science Fund of the Republic of Serbia, grant No. 7739645 “Automated sensing system based on fractal, textural and wavelet computational methods for detection of low-level cellular damage”, SensoFracTW. We also acknowledge the support of the Ministry of Education and Science of the Republic of Serbia (Grant No. 200110). Support for this project was also provided by Khalifa University of Science and Technology, Grant Numbers: FSU-2020-25 and RC2-2018-022 (HEIC), and the College of Medicine and Health Sciences, Abu Dhabi, United Arab Emirates.

**Data Availability Statement:** The data presented in this study are available on request from the corresponding author.

**Conflicts of Interest:** The authors declare no conflict of interest.

## References

- de Mattos, A.C.; Florindo, J.B.; Adam, R.L.; Lorand-Metze, I.; Metze, K. The Fractal Dimension Suggests Two Chromatin Configurations in Small Cell Neuroendocrine Lung Cancer and Is an Independent Unfavorable Prognostic Factor for Overall Survival. *Microsc. Microanal.* **2022**, *28*, 522–526. [\[CrossRef\]](#)
- De Mello, M.R.B.; Albuquerque, D.M.; Pereira-Cunha, F.G.; Albanez, K.B.; Pagnano, K.B.B.; Costa, F.F.; Metze, K.; Lorand-Metze, I. Molecular characteristics and chromatin texture features in acute promyelocytic leukemia. *Diagn. Pathol.* **2012**, *7*, 75. [\[CrossRef\]](#) [\[PubMed\]](#)
- Gupta, S.; Savala, R.; Gupta, N.; Dey, P. Fractal dimension and chromatin textural analysis to differentiate follicular carcinoma and adenoma on fine needle aspiration cytology. *Cytopathology* **2020**, *31*, 491–493. [\[CrossRef\]](#) [\[PubMed\]](#)
- Dinčić, M.; Popović, T.B.; Kojadinović, M.; Trbovich, A.M.; Ilić, A. Morphological, fractal, and textural features for the blood cell classification: The case of acute myeloid leukemia. *Eur. Biophys. J.* **2021**, *50*, 1111–1127. [\[CrossRef\]](#) [\[PubMed\]](#)
- Pantic, I.; Valjarevic, S.; Cumic, J.; Paunkovic, I.; Terzic, T.; Corridon, P.R. Gray Level Co-Occurrence Matrix, Fractal and Wavelet Analyses of Discrete Changes in Cell Nuclear Structure following Osmotic Stress: Focus on Machine Learning Methods. *Fractal Fract.* **2023**, *7*, 272. [\[CrossRef\]](#)
- Battalapalli, D.; Vidyadharan, S.; Rao, B.V.V.S.N.P.; Yogeewari, P.; Kesavadas, C.; Rajagopalan, V. Fractal dimension: Analyzing its potential as a neuroimaging biomarker for brain tumor diagnosis using machine learning. *Front. Physiol.* **2023**, *14*, 1201617. [\[CrossRef\]](#)
- Moldovanu, S.; Michis, F.A.D.; Biswas, K.C.; Culea-Florescu, A.; Moraru, L. Skin Lesion Classification Based on Surface Fractal Dimensions and Statistical Color Cluster Features Using an Ensemble of Machine Learning Techniques. *Cancers* **2021**, *13*, 5256. [\[CrossRef\]](#)
- Pantic, I.V.; Cumic, J.; Valjarevic, S.; Shakeel, A.; Wang, X.; Vurivi, H.; Daoud, S.; Chan, V.; Petroianu, G.A.; Shibru, M.G.; et al. Computational approaches for evaluating morphological changes in the corneal stroma associated with decellularization. *Front. Bioeng. Biotechnol.* **2023**, *11*, 1105377. [\[CrossRef\]](#)
- Sarica, A.; Cerasa, A.; Quattrone, A. Random Forest Algorithm for the Classification of Neuroimaging Data in Alzheimer's Disease: A Systematic Review. *Front. Aging Neurosci.* **2017**, *9*, 329. [\[CrossRef\]](#)

10. Tavus, B.; Kocaman, S.; Gokceoglu, C. Flood damage assessment with Sentinel-1 and Sentinel-2 data after Sardoba dam break with GLCM features and Random Forest method. *Sci. Total Environ.* **2022**, *816*, 151585. [\[CrossRef\]](#)
11. Yifan, C.; Jianfeng, S.; Jun, P. Development and Validation of a Random Forest Diagnostic Model of Acute Myocardial Infarction Based on Ferroptosis-Related Genes in Circulating Endothelial Cells. *Front. Cardiovasc. Med.* **2021**, *8*, 663509. [\[CrossRef\]](#)
12. Godbin, A.B.; Jasmine, S.G. Screening of COVID-19 Based on GLCM Features from CT Images Using Machine Learning Classifiers. *SN Comput. Sci.* **2022**, *4*, 133. [\[CrossRef\]](#)
13. Nikolovski, D.; Cumic, J.; Pantic, I. Application of Gray Level co-Occurrence Matrix Algorithm for Detection of Discrete Structural Changes in Cell Nuclei after Exposure to Iron Oxide Nanoparticles and 6-Hydroxydopamine. *Microsc. Microanal.* **2019**, *25*, 982–988. [\[CrossRef\]](#) [\[PubMed\]](#)
14. Karperien, A. FracLac for ImageJ. 1999–2023. Available online: <http://rsb.info.nih.gov/ij/plugins/fractal/FLHelp/Introduction.htm> (accessed on 28 January 2023).
15. Schneider, C.A.; Rasband, W.S.; Eliceiri, K.W. NIH Image to ImageJ: 25 years of image analysis. *Nature Methods* **2012**, *9*, 671–675. [\[CrossRef\]](#) [\[PubMed\]](#)
16. Basavarajappa, S.; Ramachandra, V.K.; Kumar, S. Fractal dimension and lacunarity analysis of mandibular bone on digital panoramic radiographs of tobacco users. *J. Dent. Res. Dent. Clin. Dent. Prospect.* **2021**, *15*, 140–146. [\[CrossRef\]](#) [\[PubMed\]](#)
17. da Silva, L.G.; da Silva Monteiro, W.R.S.; de Aguiar Moreira, T.M.; Rabelo, M.A.E.; de Assis, E.; de Souza, G.T. Fractal dimension analysis as an easy computational approach to improve breast cancer histopathological diagnosis. *Appl. Microsc.* **2021**, *51*, 6. [\[CrossRef\]](#) [\[PubMed\]](#)
18. Mancini, M.; Bargiacchi, L.; De Vitis, C.; D’ascanio, M.; De Dominicis, C.; Ibrahim, M.; Rendina, E.A.; Ricci, A.; Di Napoli, A.; Mancini, R.; et al. Histologic Analysis of Idiopathic Pulmonary Fibrosis by Morphometric and Fractal Analysis. *Biomedicines* **2023**, *11*, 1483. [\[CrossRef\]](#) [\[PubMed\]](#)
19. Pedregosa, F.; Varoquaux, G.; Gramfort, A.; Michel, V.; Thirion, B.; Grisel, O.; Duchesnay, É. Scikit-learn: Machine Learning in Python. *J. Mach. Learn. Res.* **2011**, *12*, 2825–2830.
20. Pantic, I.; Cumic, J.; Dugalic, S.; Petroianu, G.A.; Corridon, P.R. Gray level co-occurrence matrix and wavelet analyses reveal discrete changes in proximal tubule cell nuclei after mild acute kidney injury. *Sci. Rep.* **2023**, *13*, 4025. [\[CrossRef\]](#)
21. Metze, K.; Adam, R.; Florindo, J.B. The fractal dimension of chromatin—a potential molecular marker for carcinogenesis, tumor progression and prognosis. *Expert Rev. Mol. Diagn.* **2019**, *19*, 299–312. [\[CrossRef\]](#)
22. Panda, S.; Rahman, J.; Panigrahi, S.; Mohanty, N.; Swarnkar, T.; Mishra, U. Perspective of nuclear fractal dimension in diagnosis and prognosis of oral squamous cell carcinoma. *J. Oral. Maxillofac. Pathol.* **2022**, *26*, 127. [\[CrossRef\]](#) [\[PubMed\]](#)
23. Todorović, J.; Dinčić, M.; Nešović Ostojić, J.; Zaletel, I.; Lopičić, S.; Dundjerović, D.; Tatić, S.; Kovačević, S.; Paunović, I.; Puškaš, N.; et al. Differences in Chromatin Texture and Nuclear Fractal Dimension Between Hashimoto’s and Lymphocytic Thyroiditis Lymphocytes. *Microsc. Microanal.* **2019**, *25*, 762–768. [\[CrossRef\]](#) [\[PubMed\]](#)
24. Bouchatta, O.; Manouze, H.; Bouali-Benazzouz, R.; Kerekes, N.; Ba-M’hamed, S.; Fossat, P.; Landry, M.; Bennis, M. Neonatal 6-OHDA lesion model in mouse induces Attention-Deficit/Hyperactivity Disorder (ADHD)-like behaviour. *Sci. Rep.* **2018**, *8*, 15349. [\[CrossRef\]](#) [\[PubMed\]](#)
25. Hsu, S.; Hsu, P.; Chang, W.; Yu, C.; Wang, Y.; Yang, J.; Tsai, F.; Chen, K.; Tsai, C.; Bau, D. Protective effects of valproic acid on 6-hydroxydopamine-induced neuroinjury. *Environ. Toxicol.* **2020**, *35*, 840–848. [\[CrossRef\]](#) [\[PubMed\]](#)
26. Pantic, I.; Cumic, J.; Skodric, S.R.; Dugalic, S.; Brodski, C. Oxidopamine and oxidative stress: Recent advances in experimental physiology and pharmacology. *Chem. Biol. Interact.* **2021**, *336*, 109380. [\[CrossRef\]](#)
27. Tieu, K. A guide to neurotoxic animal models of Parkinson’s disease. *Cold Spring Harb. Perspect. Med.* **2011**, *1*, a009316. [\[CrossRef\]](#)
28. Bonilla-Porras, A.R.; Jimenez-Del-Rio, M.; Velez-Pardo, C. N-acetyl-cysteine blunts 6-hydroxydopamine- and l-buthionine-sulfoximine-induced apoptosis in human mesenchymal stromal cells. *Mol. Biol. Rep.* **2019**, *46*, 4423–4435. [\[CrossRef\]](#)
29. Schottlender, N.; Gottfried, I.; Ashery, U. Hyperbaric Oxygen Treatment: Effects on Mitochondrial Function and Oxidative Stress. *Biomolecules* **2021**, *11*, 1827. [\[CrossRef\]](#)
30. Tai, S.; Zheng, Q.; Zhai, S.; Cai, T.; Xu, L.; Yang, L.; Jiao, L.; Zhang, C. Alpha-Lipoic Acid Mediates Clearance of Iron Accumulation by Regulating Iron Metabolism in a Parkinson’s Disease Model Induced by 6-OHDA. *Front. Neurosci.* **2020**, *14*, 612. [\[CrossRef\]](#)
31. Verma, N.; Singh, H.; Khanna, D.; Rana, P.S.; Bhadada, S.K. Classification of drug molecules for oxidative stress signalling pathway. *IET Syst. Biol.* **2019**, *13*, 243–250. [\[CrossRef\]](#)
32. Pantic, I.; Paunovic, J.; Cumic, J.; Valjarevic, S.; Petroianu, G.A.; Corridon, P.R. Artificial neural networks in contemporary toxicology research. *Chem. Interact.* **2023**, *369*, 110269. [\[CrossRef\]](#) [\[PubMed\]](#)
33. Davidovic, L.M.; Cumic, J.; Dugalic, S.; Vicentic, S.; Sevarac, Z.; Petroianu, G.; Corridon, P.; Pantic, I. Gray-Level Co-occurrence Matrix Analysis for the Detection of Discrete, Ethanol-Induced, Structural Changes in Cell Nuclei: An Artificial Intelligence Approach. *Microsc. Microanal.* **2021**, *28*, 265–271. [\[CrossRef\]](#) [\[PubMed\]](#)

**Disclaimer/Publisher’s Note:** The statements, opinions and data contained in all publications are solely those of the individual author(s) and contributor(s) and not of MDPI and/or the editor(s). MDPI and/or the editor(s) disclaim responsibility for any injury to people or property resulting from any ideas, methods, instructions or products referred to in the content.